

Heat flux and wall shear stress in large-aspect-ratio turbulent vertical convection

Emily S. C. Ching ^{*}

Department of Physics, The Chinese University of Hong Kong, Shatin, Hong Kong



(Received 8 September 2022; accepted 20 January 2023; published 2 February 2023)

We present a theoretical analysis of large-aspect-ratio turbulent vertical convection that yields two relationships between heat flux and wall shear stress, measured respectively by the Nusselt number (Nu) and shear Reynolds number (Re_τ), in terms of the Rayleigh (Ra) and Prandtl numbers (Pr): $Re_\tau^2 Nu = f(\text{Pr})\text{Pr}^{-1}\text{Ra}$ in the high-Ra limit and $Nu \approx C\text{Pr}^\varepsilon Re_\tau$ with $\varepsilon = 1/3$ for $\text{Pr} \gg 1$ and $\varepsilon = 1$ for $\text{Pr} \ll 1$, where $f(\text{Pr})$ is not a power law of Pr and C is a constant. These relationships imply $Nu \approx [C^2 f(\text{Pr})]^{1/3} \text{Pr}^{-(1-2\varepsilon)/3} \text{Ra}^{1/3}$ and $Re_\tau \approx [f(\text{Pr})/C]^{1/3} \text{Pr}^{-(1+\varepsilon)/3} \text{Ra}^{1/3}$ for high Ra.

DOI: [10.1103/PhysRevFluids.8.L022601](https://doi.org/10.1103/PhysRevFluids.8.L022601)

In astrophysical, geophysical, and industrial fluid flows, fluid motions are often driven thermally by temperature differences. There are two common model systems for thermally driven flows: Rayleigh-Bénard convection in a fluid heated from below and cooled from above (see, e.g., Refs. [1–4]) and vertical convection in a fluid between two vertical walls as shown in Fig. 1. In these two systems, the direction of gravity makes a different angle to the boundaries that have a temperature difference. One important question in the study of thermally driven fluid flows is how the heat transfer depends on the control parameters of the flow. Heat flux is commonly measured by the Nusselt number (Nu) and the control parameters include the Rayleigh number $Ra \equiv \alpha g \Delta H^3 / (\nu \kappa)$, which measures the strength of thermal forcing, and the Prandtl number of the fluid $\text{Pr} \equiv \nu / \kappa$. Here, H is the separation between the two boundaries with a temperature difference Δ ; g is the acceleration due to gravity; and α , ν , and κ are the thermal expansion coefficient, kinematic viscosity, and thermal diffusivity of the fluid, respectively. A scaling theory has been developed by Grossmann and Lohse [5–8] which has successfully accounted for $Nu(\text{Ra}, \text{Pr})$ for a wide range of Ra and Pr in Rayleigh-Bénard convection. In this Letter, we study vertical convection, which is much less studied than Rayleigh-Bénard convection. Besides fundamental interest, vertical convection has many applications in engineering such as ventilation of buildings, thermal insulation in double-pane windows, and cooling of electronic devices. It also plays a crucial role in ice-ocean interactions in which fluid motion is driven by temperature difference as well as the salinity difference between the melt water and the salty seawater [9,10]. For laminar vertical convection, analysis of the steady-state boundary-layer equations gives $Nu \sim Ra^{1/4}$ [11–14] and the dependence of Nu on Pr in the low- and high-Pr limits [14]. When the flow becomes turbulent, fluctuations cannot be neglected, and a theoretical understanding of the dependence of Nu on the control parameters is yet to be attained.

Turbulent vertical convection has been investigated experimentally and by direct numerical simulations (DNS). In most of these studies, Pr is kept fixed and a range of Ra is studied. The dependence of Nu on Ra has often been reported in the form of a power law: $Nu \sim Ra^\beta$. Experimental studies for a variety of fluids showed that β changes from 1/4, the value determined for laminar flow, to 1/3 when the flow becomes turbulent [15–18]. Results consistent with $\beta = 1/3$

^{*}ching@phy.cuhk.edu.hk

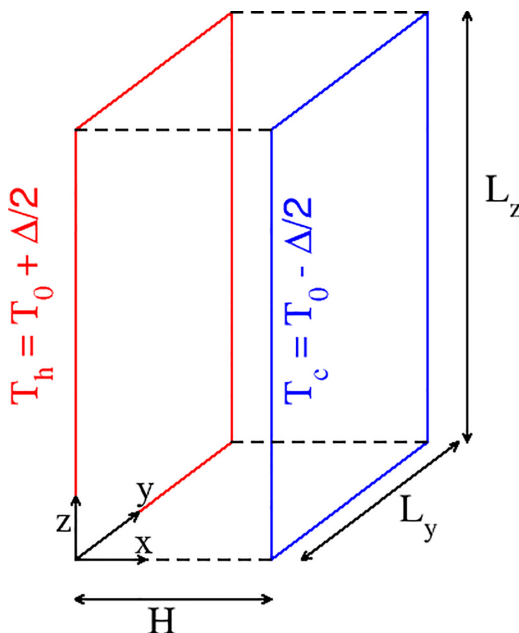


FIG. 1. A schematic diagram of vertical convection. The left vertical wall is heated while the right vertical wall is cooled, and the temperature difference is $\Delta = T_h - T_c$.

have been found in DNS in three dimensions with periodic boundary conditions in the spanwise (y) and streamwise (z) directions for $\text{Pr} = 0.709$ (air) and Ra between 10^5 and 10^7 [19,20], but other values of β were reported in DNS at the same value of Pr , such as $\beta = 1/3.2$ for a similar range of Ra [21] and $\beta = 0.31$ for a larger range of Ra up to 10^9 [22]. It was pointed out that the value of β depends on the range of Ra and $\text{Nu}(\text{Ra})$ may not be a pure power law [22]. The dependence on Pr has also been investigated for $1 \leq \text{Pr} \leq 100$ and $10^6 \leq \text{Ra} \leq 10^9$, and an effective power-law dependence of Nu on both Ra (with $\beta = 0.321$) and Pr was reported [23]. Effective power-law dependence Ra and Pr have also been reported for the wall shear stress and the maximum mean vertical velocity of the convective flow [23]. For DNS in two dimensions with adiabatic boundary condition in the horizontal boundaries, β has been found to be closer to $1/4$ than $1/3$ for $\text{Pr} = 0.71$ and $6 \times 10^8 \leq \text{Ra} \leq 10^{10}$ [24,25], but a recent study at $\text{Pr} = 10$ and Ra up to 10^{14} shows that there is a sharp transition from $\beta = 1/4$ to $\beta = 1/3$ when $\text{Ra} \geq 5 \times 10^{10}$ [26]. There have been different theoretical attempts to understand turbulent vertical convection. One approach is to identify relevant length, velocity, and temperature scales in different flow regions and develop scaling functions of velocity and temperature in each region [27–30]. By matching the scaling functions of temperature in an assumed overlap region of two flow regions, expressions for $\text{Nu}(\text{Ra})$ can be obtained and different results have been reported [27,29]. Another study has tried to extend the scaling theory of Grossmann and Lohse [5–8] for Rayleigh-Bénard convection to vertical convection but found that this approach is not feasible [22].

In this Letter, we present a theoretical analysis that yields two relationships between heat flux and wall shear stress and their dependence on Ra and Pr in the high- Ra limit. We test the theoretical results for high Pr against the openly available DNS data for $1 \leq \text{Pr} \leq 100$ and $10^6 \leq \text{Ra} \leq 10^9$ [23] and find excellent agreement.

We consider a fluid confined between two vertical walls, with the left wall heated at a temperature T_h and the right wall cooled at a temperature T_c , and the temperature difference Δ is equal to $T_h - T_c$ (see Fig. 1). With the Oberbeck-Boussinesq approximation, which neglects the variation of temperature in the fluid for all purposes except for the determination of the buoyancy force, the

governing equations are

$$\frac{\partial \mathbf{u}}{\partial t} + \mathbf{u} \cdot \nabla \mathbf{u} = -\frac{1}{\rho} \nabla p + \nu \nabla^2 \mathbf{u} + \alpha g (T - T_0) \hat{z} \quad (1)$$

$$\frac{\partial T}{\partial t} + \mathbf{u} \cdot \nabla T = \kappa \nabla^2 T \quad (2)$$

$$\nabla \cdot \mathbf{u} = 0, \quad (3)$$

where $\mathbf{u}(x, y, z, t) = (u, v, w)$ is the velocity, $p(x, y, z, t)$ the pressure, $T(x, y, z, t)$ the temperature, T_0 the average temperature of the two vertical plates, and ρ the density of the fluid at $T = T_0$. The coordinate system is shown in Fig. 1 and \hat{z} is a unit vector along the vertical direction. The velocity field satisfies the no-slip boundary condition at the two vertical plates. The flow quantities are Reynolds decomposed into sums of time averages and fluctuations, e.g., $u(x, y, z, t) = U(x, y, z) + u'(x, y, z, t)$ and $T(x, y, z, t) - T_0 = \Theta(x, y, z) + \theta'(x, y, z, t)$. We focus at the large-aspect-ratio limit, namely, $L_z/H \gg 1$ and $L_y/H \gg 1$, where L_z and L_y are the height and width of the vertical walls. In this limit, all the mean flow quantities depend on x only. Using the continuity equation Eq. (3) and the no-slip boundary condition, we obtain $U = 0$. Taking the time average of Eqs. (1) and (2) leads to the mean momentum balance and mean thermal energy balance equations [19],

$$\frac{d}{dx} \langle u'w' \rangle_t = \nu \frac{d^2}{dx^2} W + \alpha g \Theta \quad (4)$$

$$\frac{d}{dx} \langle u'\theta' \rangle_t = \kappa \frac{d^2}{dx^2} \Theta, \quad (5)$$

where $\langle \dots \rangle_t$ denotes an average over time. In DNS where the computational domain is finite, the same equations can be derived for the mean quantities averaged over time as well as over y and z if periodic boundary conditions are enforced in the y and z directions [23]. Due to the symmetry of the problem, the mean velocity and temperature profiles $W(x)$ and $\Theta(x)$ are antisymmetric about $x = H/2$, thus one only has to study Eqs. (4) and (5) for $0 \leq x \leq H/2$. The boundary conditions are

$$W(0) = W(H/2) = \Theta(H/2) = 0; \quad \Theta(0) = \Delta/2. \quad (6)$$

Integrating Eq. (5) with respect to x , one obtains

$$\langle u'\theta' \rangle_t - \kappa \frac{d\Theta}{dx} = -\kappa \frac{d\Theta}{dx} \Big|_{x=0}, \quad (7)$$

showing that the mean horizontal heat flux $Q = \rho c \langle u'\theta' \rangle_t - k d\Theta/dx$ along the x direction is independent of x [27]. Here, c and k are the specific heat capacity and thermal conductivity of the fluid, respectively. Nu is defined as the ratio of actual heat flux to that when there was only thermal conduction, thus

$$\text{Nu} \equiv \frac{Q}{k\Delta/H} = -\frac{d\Theta}{dx} \Big|_{x=0} \frac{H}{\Delta} = \frac{H}{2\delta_T}, \quad (8)$$

where δ_T is the thermal boundary layer thickness defined by $\delta_T \equiv k\Delta/(2Q)$. Integrating Eq. (4) with respect to x gives [27]

$$\langle u'w' \rangle_t = \nu \frac{dW}{dx} + \alpha g \int_0^x \Theta(x') dx' - \nu \frac{dW}{dx} \Big|_{x=0}. \quad (9)$$

The wall shear stress is given by $\tau_w = \rho \nu dW/dx|_{x=0}$ and is often measured by the dimensionless shear Reynolds number $\text{Re}_\tau \equiv u_\tau H/\nu$ in terms of the friction velocity $u_\tau \equiv \sqrt{\nu dW/dx|_{x=0}}$. If $W(x)$ and $\Theta(x)$ could be solved, then their gradients at $x = 0$ or, equivalently, Re_τ and Nu would be obtained, but Eqs. (4) and (5) are not closed due to the presence of the second-order correlations

$\langle u'w' \rangle_t$ and $\langle u'\theta' \rangle_t$. This is the well-known closure problem of turbulence in which there are more unknowns than equations. Our first step to tackle this problem is to evaluate Eq. (9) at $x = x_0$, the location at which the magnitudes of the Reynolds shear stress and viscous stress are equal, i.e., $\nu dW/dx|_{x=x_0} = \langle u'w' \rangle_t(x_0)$. Near the wall, the viscous stress $\rho \nu dW/dx$ dominates over the Reynolds shear stress $-\rho \langle u'w' \rangle_t$, which is small and positive. As one moves away from the wall, the viscous stress decreases while the Reynolds shear stress becomes negative and increases in magnitude. Towards the centerline $x = H/2$, the viscous stress becomes negative and the magnitude of the Reynolds shear stress dominates over that of the viscous stress. The magnitudes of the two stresses are equal at $x = x_0$. Evaluating Eq. (9) at $x = x_0$ thus bypasses the difficulty of estimating $\langle u'w' \rangle_t$ and gives

$$\nu \frac{dW}{dx} \Big|_{x=0} = \alpha g \int_0^{x_0} \Theta(x') dx'. \quad (10)$$

Equation (10) shows explicitly that the wall shear stress τ_w is generated by buoyancy and is equal to the buoyancy force per unit area within the velocity boundary layer with $x \leq x_0$. We define a dimensionless temperature function $\Phi(\xi)$ of $\xi \equiv x/\delta_T$ by

$$\Theta(x = \xi \delta_T) \equiv \Delta \Phi(\xi)/2 \quad (11)$$

and rewrite Eq. (10) to yield a universal relation between Re_τ and Nu :

$$\text{Re}_\tau^2 \text{NuPrRa}^{-1} = \frac{1}{4} \int_0^{\xi_0} \Phi(\xi) d\xi \equiv I(\text{Ra}, \text{Pr}), \quad (12)$$

where $\xi_0 = x_0/\delta_T$. Using Eqs. (6) and (8), we obtain the boundary conditions for Φ :

$$\Phi(0) = 1, \quad \Phi(\text{Nu}) = 0, \quad \Phi'(0) = -1. \quad (13)$$

We evaluate $\Phi(\xi)$ and ξ_0 using the DNS data from Howland *et al.* [23,31] to study the Ra and Pr dependence of the integral I . As shown in Fig. 2, $\Phi(\xi)$ approaches an asymptotic form in the high-Ra limit for each Pr, and the asymptotic form depends on Pr. In Fig. 3 it can be seen that ξ_0 increases slowly with Ra for each Pr. Since $\Phi(\xi)$ decreases to zero for large ξ , these results suggest that the integral I tends to a Ra-independent function $f(\text{Pr})$ in the high-Ra limit. The available DNS data cover $1 \leq \text{Pr} \leq 100$, but we expect $\Phi(\xi)$ to approach an asymptotic form for general Pr. For $\text{Pr} < 1$, as the velocity boundary layer is nested within the thermal boundary layer, ξ_0 has to be less than 1 and thus cannot increase with Ra asymptotically. It is expected that ξ_0 approaches a constant in the high-Ra limit for $\text{Pr} < 1$ and $I(\text{Ra}, \text{Pr}) \rightarrow f(\text{Pr})$ also for $\text{Pr} < 1$. Hence, we assume that

$$\text{Re}_\tau^2 \text{NuPrRa}^{-1} = f(\text{Pr}) \quad \text{high-Ra limit.} \quad (14)$$

We estimate the values of $f(\text{Pr})$ from the DNS data [23] as follows. Among the 38 sets of data, most data were taken at $\text{Pr} = 10$. Thus, we take $f_0 \equiv f(\text{Pr} = 10)$ as a reference and estimate the values of $f(\text{Pr})/f_0$ by the averages of the ratio of the data points $\text{Re}_\tau^2 \text{NuPrRa}^{-1}$ for each of the other values of Pr to the data points at $\text{Pr} = 10$, taken at the seven common values of Ra. The errors of the estimated $f(\text{Pr})/f_0$ are measured by the standard deviations. Equation (14) implies that the data points of $\text{Re}_\tau^2 \text{Nu}$ for different values of Pr, when multiplied by $\text{Pr}f_0/f(\text{Pr})$, would collapse into a single curve of $f_0 \text{Ra}$ for large Ra. This is confirmed in Fig. 4, and as shown in the right inset of Fig. 4, $f(\text{Pr})/f_0$ cannot be approximated by a power law. Using Eqs. (8) and (11), we rewrite Eq. (7) as

$$\frac{\langle u'\theta' \rangle_t}{\nu \Delta/H} = \text{NuPr}^{-1} [1 + \Phi'(\xi)]. \quad (15)$$

Because of the boundary conditions, u' , θ' , and $\partial u'/\partial x = -(\partial v'/\partial y + \partial w'/\partial z)$ vanish at $x = 0$. As a result, $\langle u'\theta' \rangle_t$ and its first- and second-order derivatives with respect to x vanish at $x = 0$, while

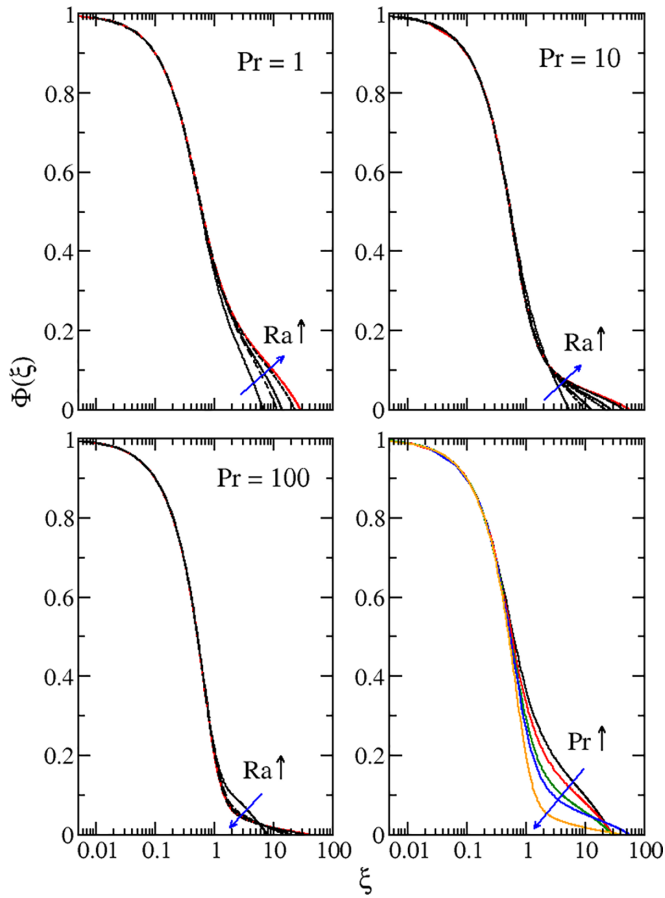


FIG. 2. Plots of $\Phi(\xi)$ vs x showing its dependence on Ra for $Pr = 1, 10, 100$ and its dependence on Pr at the largest Ra (10^8 for $Pr = 1, 2, 5$ and 10^9 for $Pr = 10, 100$) using DNS data from Howland *et al.* [23].

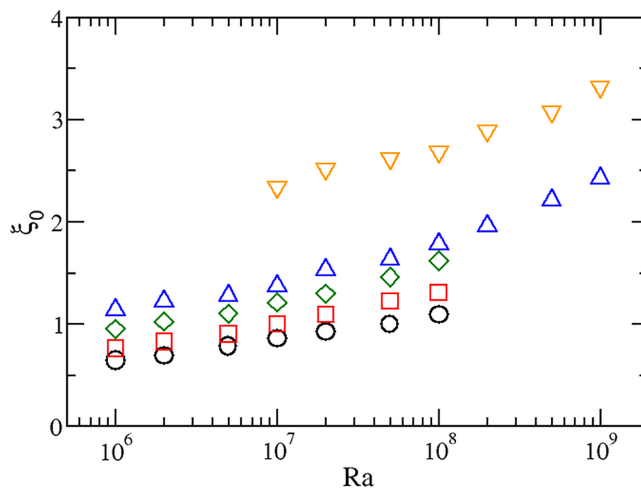


FIG. 3. Dependence of ξ_0 on Ra for $Pr = 1$ (circles), 2 (squares), 5 (diamonds), 10 (triangles), and 100 (inverted triangles).

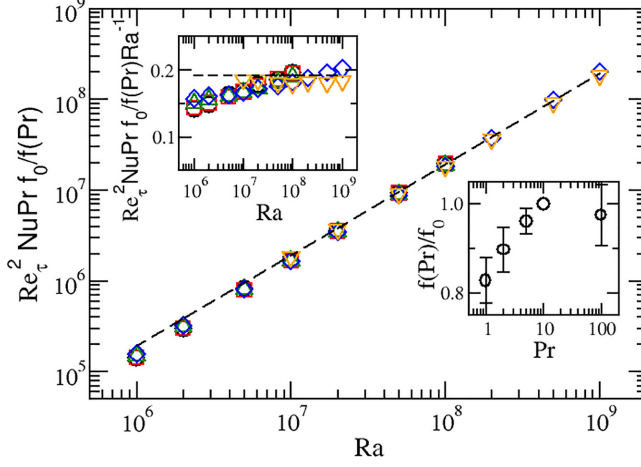


FIG. 4. Dependence of $\text{Re}_\tau^2 \text{Nu Pr } f_0 / f(\text{Pr})$ on Ra using the DNS data [23] for $\text{Pr} = 1, 2, 5, 10, 100$ with same symbols as in Fig. 3. The dashed line is the best fit of the data points for $\text{Ra} \geq 5 \times 10^7$ by the function $y = ax$, and the fitted value of a gives $f_0 = 0.19$. The inset on the left shows the compensated plots while the inset on the right shows $f(\text{Pr})/f_0$ vs Pr .

$d^3 \langle u' \theta' \rangle_t / dx^3 |_{x=0} = 3 \langle (\partial^2 u' / \partial x^2) (\partial \theta' / \partial x) \rangle_t |_{x=0}$. Taking the third-order derivative of Eq. (15) with respect to ξ at $\xi = 0$ gives

$$\frac{3H^4}{8\nu\Delta} \text{Nu}^{-3} \left\langle \frac{\partial^2 u'}{\partial x^2} \frac{\partial \theta'}{\partial x} \right\rangle_t \Big|_{x=0} = \text{Nu Pr}^{-1} \Phi^{(4)}(0). \quad (16)$$

Next, we make a closure estimate of $\langle (\partial^2 u' / \partial x^2) (\partial \theta' / \partial x) \rangle_t |_{x=0}$. Physically we expect it to be related to the wall shear stress τ_w and the heat flux Q and, therefore depends on u_τ and $-d\Theta/dx|_{x=0}$. Near the wall, the molecular diffusivities are significant and we take the characteristic length scale to be $l_c = \nu/u_\tau$ for $\text{Pr} \gg 1$ and $l_c = \kappa/u_\tau$ for $\text{Pr} \ll 1$. Thus, we let $\langle (\partial^2 u' / \partial x^2) (\partial \theta' / \partial x) \rangle_t |_{x=0} = F(u_\tau, -d\Theta/dx|_{x=0}, l_c)$ and estimate the function F by dimensional analysis to obtain

$$\left\langle \frac{\partial^2 u'}{\partial x^2} \frac{\partial \theta'}{\partial x} \right\rangle_t \Big|_{x=0} \approx c_0 \frac{u_\tau}{l_c^2} \frac{\text{Nu} \Delta}{H}. \quad (17)$$

We have used Eq. (8) to write $-d\Theta/dx|_{x=0} = \text{Nu} \Delta / H$. Substituting Eq. (17) into Eq. (16), we obtain

$$\text{Nu} \approx C \text{Pr}^\varepsilon \text{Re}_\tau, \quad \varepsilon = \begin{cases} 1/3 & \text{Pr} \gg 1 \\ 1 & \text{Pr} \ll 1, \end{cases} \quad (18)$$

where $C = \{3c_0/[8\Phi^{(4)}(0)]\}^{1/3}$ is approximated as a constant, neglecting the possible weak Pr dependence of $\Phi^{(4)}(0)$. Equation (18) for $\text{Pr} \gg 1$ agrees with the numerical result $\text{Nu} \sim \text{Pr}^{1/3} \text{Re}_\tau$ found for $1 \leq \text{Pr} \leq 100$ [23]. A relationship $\text{Nu} \propto [\gamma(\text{Pr})\text{Pr}]^{1/3} \text{Re}_\tau$, where $\gamma(\text{Pr})$ is an undetermined function of Pr , has been obtained for high Pr by assuming that the eddy diffusivity, defined by $-\langle u' \theta' \rangle_t / (\partial \Theta / \partial x)$, can be approximated by a cubic function of x , $\gamma(\text{Pr}) u_\tau^3 x^3 / \nu^2$, throughout the thermal boundary layer [32] but the cubic-function approximation is valid only for a very small region close to the wall and does not hold for the whole thermal boundary layer.

Solving Eqs. (14) and (18), we obtain

$$\text{Nu} \approx [C^2 f(\text{Pr})]^{1/3} \text{Pr}^{-(1-2\varepsilon)/3} \text{Ra}^{1/3} \quad (19)$$

$$\text{Re}_\tau \approx [f(\text{Pr})/C]^{1/3} \text{Pr}^{-(1+\varepsilon)/3} \text{Ra}^{1/3} \quad (20)$$

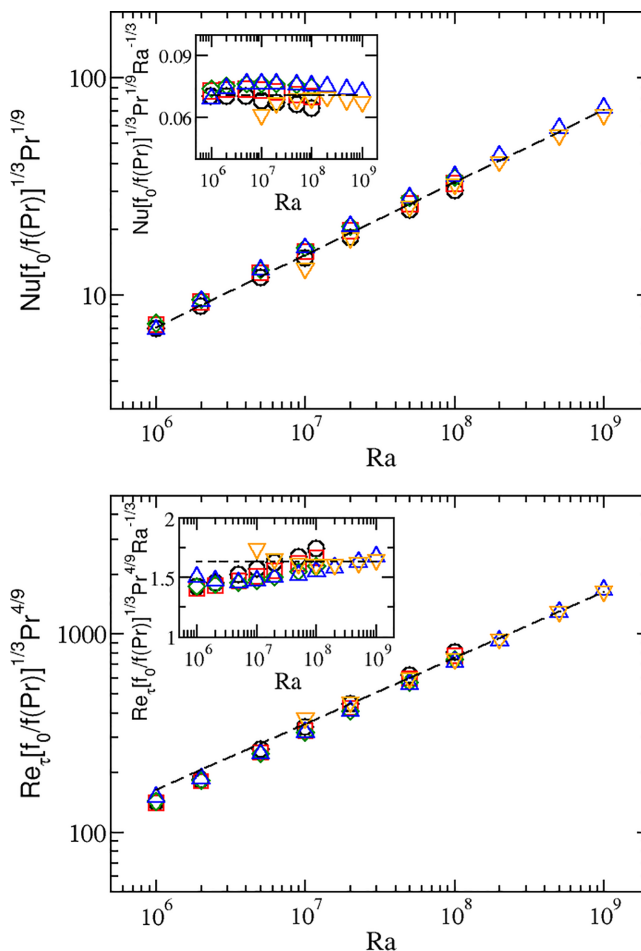


FIG. 5. Dependence of $\text{Nu}[f_0/f(\text{Pr})]^{1/3}\text{Pr}^{1/9}$ (top) and $\text{Re}_\tau[f_0/f(\text{Pr})]^{1/3}\text{Pr}^{4/9}$ (bottom) on Ra using the DNS data [23] for $\text{Pr} = 1, 2, 5, 10, 100$ with the same symbols as in Fig. 3. The dashed lines are the best fits of the theoretical prediction $y \propto x^{1/3}$ for data points taken at $\text{Ra} \geq 5 \times 10^7$, and the fitted values of the proportionality constants in the two fits give $f_0 = 0.19$ and $C = 0.043$. The insets show the compensated plots.

in the high- Ra limit. These theoretical results imply that data points of Nu and Re_τ taken at different values of Pr can be collapsed into single curves of $\text{Ra}^{1/3}$ dependence for large Ra when multiplied by appropriate factors of $f(\text{Pr})$ and Pr . As shown in Fig. 5, the theoretical predictions for high Pr are in excellent agreement with the available DNS data for $1 \leq \text{Pr} \leq 100$ [23]. Data for low Pr and high Ra are not yet available.

In summary, we have obtained theoretical results for the dependence of Nu and Re_τ on Ra and Pr , answering the question of how heat flux and wall shear stress depend on the control parameters for large-aspect-ratio turbulent vertical convection in the high- Ra limit. Such a question is challenging because of the underlying closure problem of turbulence in which Eqs. (4) and (5) for the mean quantities, $W(x)$ and $\Theta(x)$, contain additional unknowns of the second-order correlations, $\langle u'w' \rangle_t$ and $\langle u'\theta' \rangle_t$. Our theoretical analysis purposefully bypasses the difficulty of directly estimating $\langle u'w' \rangle_t$, assumes the integral $I(\text{Ra}, \text{Pr})$ approaching a Ra -independent function in the high- Ra limit, and makes a minimal closure estimate of the third-order derivative of $\langle u'\theta' \rangle_t$ at $x = 0$ instead of the whole function. For finite Ra , the additional Ra dependence of $I(\text{Ra}, \text{Pr})$ [see Eq. (12)], which is expected not in the form of a power law, would modify the $\text{Ra}^{1/3}$ dependence of Nu and Re_τ . This

could explain the variations of the effective power-law exponent β for $\text{Nu}(\text{Ra})$ observed in different ranges of Ra in DNS [19–23]. The present work studies the limit of large aspect ratios, but our theoretical result of $\text{Nu} \sim \text{Ra}^{1/3}$ in the high- Ra limit is also in agreement with the DNS result for a two-dimensional cell with a unit aspect ratio in the turbulent regime [26].

The author thanks C. J. Howland for providing the DNS data and D. Lohse and O. Shishkina for discussions. She also acknowledges support from the Hong Kong Research Grants Council (Grant No. CUHK 14302419).

- [1] G. Ahlers, S. Grossmann, and D. Lohse, Heat transfer and large scale dynamics in turbulent Rayleigh–Bénard convection, *Rev. Mod. Phys.* **81**, 503 (2009).
- [2] D. Lohse and K.-Q. Xia, Small-scale properties of turbulent Rayleigh–Bénard convection, *Annu. Rev. Fluid Mech.* **42**, 335 (2010).
- [3] F. Chillà and J. Schumacher, New perspectives in turbulent Rayleigh–Bénard convection, *Eur. Phys. J. E* **35**, 58 (2012).
- [4] E. S. C. Ching, *Statistics and Scaling in Turbulent Rayleigh–Bénard Convection* (Springer, Singapore, 2014).
- [5] S. Grossmann and D. Lohse, Scaling in thermal convection: A unifying theory, *J. Fluid Mech.* **407**, 27 (2000).
- [6] S. Grossmann and D. Lohse, Thermal Convection for Large Prandtl Numbers, *Phys. Rev. Lett.* **86**, 3316 (2001).
- [7] S. Grossmann and D. Lohse, Prandtl and Rayleigh number dependence of the Reynolds number in turbulent thermal convection, *Phys. Rev. E* **66**, 016305 (2002).
- [8] S. Grossmann and D. Lohse, Fluctuations in turbulent Rayleigh–Bénard convection: The role of plumes, *Phys. Fluids* **16**, 4462 (2004).
- [9] B. Gayen, R. W. Griffiths, and R. C. Kerr, Simulation of convection at a vertical ice face dissolving into saline water, *J. Fluid Mech.* **798**, 284 (2016).
- [10] C. J. Howland, R. Verzicco, and D. Lohse, Double-diffusive transport in multicomponent vertical convection, *Phys. Rev. Fluids* **8**, 013501 (2023).
- [11] S. Ostrach, An analysis of laminar free-convection flow and heat transfer about a flat plate parallel to the direction of the generating body force, NACA Report **1111**, 63 (1953).
- [12] G. K. Batchelor, Heat transfer by free convection across a closed cavity between vertical boundaries at different temperatures, *Quart. Appl. Math.* **12**, 209 (1954).
- [13] H. K. Kuiken, An asymptotic solution for large Prandtl number free convection, *J. Eng. Math* **2**, 355 (1968).
- [14] O. Shishkina, Momentum and heat transport scalings in laminar vertical convection, *Phys. Rev. E* **93**, 051102(R) (2016).
- [15] M. Jakob, *Heat Transfer* (Wiley, New York, 1949).
- [16] R. K. MacGregor and A. F. Emery, Free convection through vertical plane layers—Moderate and high Prandtl number fluids, *Trans. ASME, J. Heat Transfer* **93**, 253 (1971).
- [17] S. W. Churchill and H. H. S. Chu, Correlating equations for laminar and turbulent free convection from a vertical plate, *Int. J. Heat Mass Transf.* **18**, 1323 (1975).
- [18] T. Tsuji and Y. Nagano, Characteristics of a turbulent natural convection boundary layer along a vertical flat plate, *Int. J. Heat Mass Transf.* **31**, 1723 (1988).
- [19] T. A. M. Versteegh and F. T. M. Nieuwstadt, A direct numerical simulation of natural convection between two infinite vertical differentially heated walls scaling laws and wall functions, *Int. J. Heat Mass Transf.* **42**, 3673 (1999).
- [20] C. S. Ng, D. Chung, and A. Ooi, Turbulent natural convection scaling in a vertical channel, *Int. J. Heat Fluid Flow* **44**, 554 (2013).

- [21] P. Kiš and H. Herwig, The near wall physics and wall functions for turbulent natural convection, [Int. J. Heat Mass Transf. **55**, 2625 \(2012\)](#).
- [22] C. S. Ng, A. Ooi, D. Lohse, and D. Chung, Vertical natural convection: Application of the unifying theory of thermal convection, [J. Fluid Mech. **764**, 349 \(2015\)](#).
- [23] C. J. Howland, C. S. Ng, R. Verzicco, and D. Lohse, Boundary layers in turbulent vertical convection at high Prandtl number, [J. Fluid Mech. **930**, A32 \(2022\)](#).
- [24] S. Xin and P. Le Quéré, Direct numerical simulations of two-dimensional chaotic natural convection in a differentially heated cavity of aspect ratio 4, [J. Fluid Mech. **304**, 87 \(1995\)](#).
- [25] F. X. Trias, M. Soria, A. Oliva, and C. D. P'erez-Segarra, Direct numerical simulations of two- and three-dimensional turbulent natural convection flows in a differentially heated cavity of aspect ratio 4, [J. Fluid Mech. **586**, 259 \(2007\)](#).
- [26] Q. Wang, H.-R. Liu, R. Verzicco, O. Shishkina, and D. Lohse, Regime transitions in thermally driven high-Rayleigh number vertical convection, [J. Fluid Mech. **917**, A6 \(2021\)](#).
- [27] W. K. George, Jr. and S. P. Capp, A theory for natural convection turbulent boundary layers next to heated vertical surfaces, [Int. J. Heat Mass Transf. **22**, 813 \(1979\)](#).
- [28] M. Hölling and H. Herwig, Asymptotic analysis of the near-wall region of turbulent natural convection flows, [J. Fluid Mech. **541**, 383 \(2005\)](#).
- [29] C. Balaji, M. Hölling, and H. Herwig, Nusselt number correlations for turbulent natural convection flows using asymptotic analysis of the near-wall region, [ASME. J. Heat Transfer **129**, 1100 \(2007\)](#).
- [30] T. Wei, Multiscaling analysis of buoyancy-driven turbulence in a differentially heated vertical channel, [Phys. Rev. Fluids **4**, 073502 \(2019\)](#).
- [31] Additional DNS data on the profiles of $\langle u'w' \rangle_t$, have been provided by Christopher J. Howland.
- [32] E. Ruckenstein and J. D. Felske, Turbulent natural convection at high Prandtl numbers, [ASME. J. Heat Transfer **102**, 773 \(1980\)](#).